Hydrostatic contraction and anisotropic contraction effects on oxygen molecule nanorods

Masaki Mito[1],* Kensuke Hario[1], Yuichiro Kitamura[1], Hiroyuki Deguchi[1], and Takayuki Tajiri[2]
[1] *Graduate School of Engineering, Kyushu Institute of Technology, Kitakyushu 804-8550, Japan and*
[2] *Faculty of Science, Fukuoka University, Fukuoka 814-0180, Japan*
(Dated: June 21, 2020)

We study the effects of both hydrostatic and anisotropic contractions on the molecular condensation of oxygen molecules (O_2) physisorbed to nanosized pores, termed "O_2 nanorods", through the magnetization measurements. Multisteps of O_2 solidification accompany the reduction in structural symmetry with decreasing temperature, such that the structural change by external stress varies the stability of O_2 solidification. For initial pore diameters of D = 8.5, 14.5, and 24.0 nm, anisotropic compression for nanorods (preferential compression along radial direction of the pores) occurred, and molecule solidification is suppressed at the lower temperature side compared with that under hydrostatic compression. For the smallest D = 6.5 nm, a hydrostatic contraction almost occurred, and the high adsorption capability enabled the detection of both the melting transition and change in crystal structure within the β phase, in addition to α–β and β–γ transitions.

PACS numbers:

I. INTRODUCTION

Oxygen molecules O_2, which comprise two oxygen atoms, exhibit magnetic properties characteristic of spin quantum number $S = 1$ [1]. When $S = 1$ spins are arranged on a low-dimensional lattice, rich magnetic properties appear in addition to molecular condensation as gas $\rightarrow$ liquid $\rightarrow$ solid. Additionally, quantum spin systems related with the Haldane problem are garnering interest [2]. Hence, O_2 is promising as a magnetic material, and its scientific history is as follows: According to the review by Freimana and Jodl [1], the paramagnetic property in gas and liquid states was first discovered by Faraday [3] in 1848 and Dewar [4] in 1891, respectively. Magnetic susceptibility measurements for condensed O_2 were initiated by Onnes and Perrier in 1910 [5]. More systematic studies were performed in the 1950's by Borovik–Romanov [6] and Kanda *et al*. [7]. In the 1980's, magnetic susceptibility for solid states were successfully measured by DeFotis in 1981 [8] and Meier *et al*. in 1982 [9]. In 1985, a magnetic measurement at a high magnetic field was performed by Uyeda *et al*. [10].

From high−temperature side, three solid phases exist: γ, β, and α phases [1, 11]. First, the cubic γ phase for 43.8–54.4 K contains two sphere molecules at 2*a* sites and six disc ones at 6*d* sites forming chains extending in three [100] directions [1]. The magnetic property of the γ phase is composed of a one-dimensional correlation and paramagnetic spins [8]. Next, the rhombohedral β phase for 23.9–43.8 K is of a two-dimensional short range order and, for 26–42 K, the tilt angle of precession motion changes [12]. Finally, the monoclinic α phase below 23.9 K has an antiferromagnetic ordering, and its lattice structure is represented by a tilted rhombohedral lattice. The β–γ transition exhibits the largest anomaly in magnetic susceptibility among the α–β, β–γ, and γ–liquid transitions. The magnitude of the discrete change in magnetic susceptibility for phase transition between solid phases is related to the change in the molar volume V; $V_{\beta-\gamma} = 0.9$ cm^3/mol, $V_{\alpha-\beta} = 0.1$ cm^3/mol (for reference, $V_{\gamma-\mathrm{liquid}} = 0.8$ cm^3/mol) [13]. Recently, a change in crystal structure at high magnetic fields has been reported [14], suggesting a prominent magneto-structural correlation.

Since the 1980's, physical measurements at high pressures have been an important aspect in O_2 molecule condensation research [1, 11]. In fact, spectroscopy and X-ray diffraction experiments have been performed extensively in the aforementioned research [1]. In 1982, Meier observed magnetic susceptibility under a high pressure up to 0.8 GPa [9]. In 2014, we performed investigations based on an enlarged pressure region, i.e., up to 3.3 GPa [15]. Because it was difficult to detect minute magnetic signals, the pressure range of magnetic susceptibility measurements has been restricted to a much lower pressure side compared with other physical measurements, such as in optical studies (132 GPa [16]), infrared spectroscopy (92 GPa [17]), Raman spectroscopy (120 GPa [18], 134 GPa [19]), X-ray diffraction (116 GPa [20], 115 GPa [18], 133 GPa [21]), electrical conductivity (125 GPa [22]), and neutron diffraction (10 GPa [23]).

Magnetic susceptibility measurements has provided only physical information restricted to β–γ and α–β transitions thus far [9, 15]. The γ phase is translationally ordered, whereas the precession motion of disc-like molecules and the rotational motion of orientationally disordered molecules occurred. Hence, in the process of $\alpha \rightarrow \beta \rightarrow \gamma \rightarrow$ liquid phases, the β–γ transition can be considered as an intermediate step to a complete disordering. Under a high pressure, the stability of the aforementioned rotations at the γ phase might be suppressed. Herein, we list up a few interests related to the present study: (1) The phase boundary between γ and

*Electronic address: mitoh@mns.kyutech.ac.jp

liquid phases at high pressures have not been determined through magnetic measurements. (2) The temperature dependence of the precession angle in the β phase at the ambient and hydrostatic pressures has not been investigated in magnetic susceptibility measurements. (3) In addition, anisotropic contraction effects on a condensed O_2 system have not been investigated thus far.

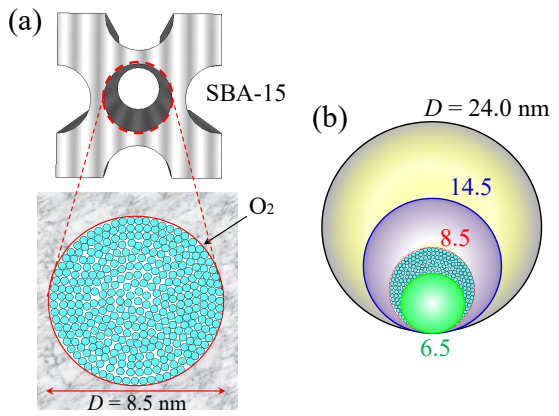

FIG. 1: (Color online) (a) Overview of O_2 physisorption into a pore of SBA-15 with pore size $D = 8.5$ nm. (b) Comparison of pore size for $D = 6.5$–24.0 nm.

To investigate the anisotropic contraction effects on condensed O_2, we used a physisorption media. O_2 gas can be physisorbed on graphite [24, 25] and boron nitride substrates [26] as well as into porous materials, such as organic-metal composite materials (pore size of 0.5–0.7 nm) [27–30], and nanoporous silica (pore size of 4 nm) [31]. Ordinal structural phase transformation of solid ($\alpha \rightarrow \beta \rightarrow \gamma$) $\rightarrow$ liquid $\rightarrow$ gas from the low temperature side also occurred in nanosized porous spaces of sufficient cross-section and volume. When the nanosized rod above was used, the hydrostatic compression for the composite of O_2 and porous material resulted in an anisotropic contraction for condensed O_2 with the rod structure; consequently, this compression affected the condensation state of O_2.

In this study, we conducted a hydrostatic pressure experiment for O_2 physisorbed into nanosized pores with $D = 6.5$–24.0 nm, in which O_2 nanorods were constructed. In fact, the pressure effects on $D = 6.5$ nm were consistent with that on the bulk system; hence, we were able to determine several phase boundaries with the best accuracy compared with other related studies owing to the high adsorption capability of a nanoporous silica SBA-15. With increasing D, the phase diagram deviated from that of the bulk system; meanwhile, for $D = 24.0$ nm, phase diagram approached that of the bulk system. Hence, we discovered the effect of compression style on O_2 condensation.

II. METHODS

Mesoporous silica, termed SBA-15, was prepared according to the literature [32–34]. The diameter of the pore (D) was evaluated by X-ray diffraction, and four types of SBA-15 with $D = 6.5$, 8.5, 14.5, and 24.0 nm, whose error was ± 0.2 nm, were prepared. The van der Waals diameter of O_2 based on the Renard-Jhonse potential is 4 Å. The aforementioned SBA-15 of $D = 6.5$, 8.5, 14.5, and 24.0 nm permits the O_2 condensation per cross section of approximately 200 (8 layers), 350 (10 layers), 1000 (18 layers), and 2800 (29 layers), respectively.

Compression corresponding to a stress of up to 3.3 GPa at room temperature was achieved using a miniature CuBe diamond anvil cell (DAC) that comprised two diamond anvils with flat tips having a diameter of 1.0 mm and a 0.25-mm-thick CuBe gasket [35, 36]. The sample cavity with the 0.6mm diameter was prepared by creating a hole in the CuBe gasket using electrical discharge machining. The powder of SBA-15 and small pieces of ruby as a manometer were installed into the sample chamber with the help of a fluorine oil (FC77), which was volatilized after its installation. After removing air in SBA-15, liquid O_2 was injected into SBA-15 set in the miniature DAC according to the method described in Ref. [15].

The DC magnetization (M) of condensed O_2 at Gigapascal pressures was measured using a superconducting quantum interference device magnetometer [15, 37–40]. The temperature T dependence of M was measured at the DC magnetic field $H = 5$ kOe after rapid cooling from room-temperature to 5 K. The pressure value at room temperature ($P_{\rm rt}$) was evaluated by measuring the fluorescence of ruby [41] located in the sample cavity. The value of $P_{\rm rt}$ was adopted as the pressure value (P) for each measurement. According to similar experiments for condensed O_2 using the same miniature DAC, for $P_{\rm rt} \geq 1.4$ GPa, it was confirmed that pressure barely depended on temperature in an experiment without SBA-15 [for $P_{\rm rt} = 1.1$ GPa, the pressure value at 50 K reduced to approximately one half of $P_{\rm rt}$] [15]. From comparing the phase diagrams for four Ds, we decided to adopt the present results for $P \geq 1.4$ GPa.

III. EXPERIMENTAL RESULTS AND DISCUSSION

A. $D = 6.5$ nm

Figure 2 shows the T dependence of M for O_2 physisorbed into the pores of SBA-15 with $D = 6.5$ nm. First, for the result based on $P = 1.8$ GPa, five characteristic anomalies due to the α–β transition, two well-unknown anomalies in the β phase, a β–γ transition, and a γ-liquid transition were observed. The anomaly due to the β–γ transition was the largest among the five anomalies, consistent with the results in the literature [9, 15].

One of two well-unknown anomalies in the β phase was observed in previous experiments [15, 31], whereas the detection of both is rare. The corresponding anomalies associated with the change in the precession angle [12] had been confirmed in the temperature dependence of the vibron bandwidth of Raman scattering [42]; furthermore, they have not been detected in the magnetic susceptibility thus far. The success in detecting these magnetic anomalies is attributed to the high adsorption from using porous materials. For $1.8 \leq P \leq 3.3$ GPa, all the anomalies can be defined, as plotted in the phase diagram of Fig. 3 together with results from a previous experiment without using SBA-15 [15]. Both the α–β and β–γ transitions were consistent with the results of a previous experiment [15]. For $D = 6.5$ nm, hydrostatic contraction occurred, and we assumed that the blockade of pore edges would occur under a compressed environment. Furthermore, the high physisorption of SBA-15 enabled the detection of the γ-liquid transition, which could not be detected in previous studies [9, 15]. The present pressure response is intrinsically consistent with that based on previous Raman experiments [1, 43–45]. Thus, the novelty of this study is the detection of two well-unknown anomalies in the β phase and that of the γ-liquid transition in magnetic susceptibility measurements.

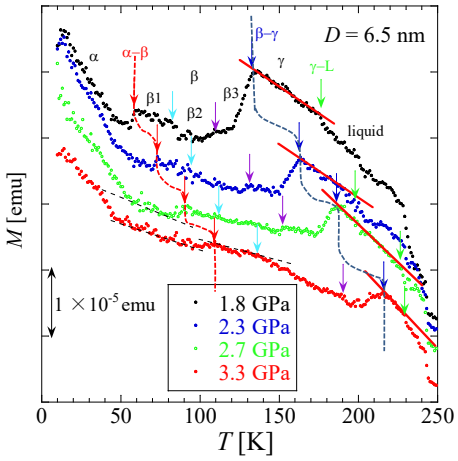

FIG. 2: (Color online) Temperature T dependence of magnetization M for oxygen molecules physisorbed into SBA-15 with $D = 6.5$ nm under compression. The characteristic temperatures for the α–β transition, two well-unknown anomalies, β–γ transition, and γ-liquid (γ-L) transition are represented in red, light blue, purple, blue, and green arrows, respectively. The anomaly around 230 K barely depended on the pressure, which was assumed to be due to the O_2 adsorption on the surface of SBA-15.

In the rhombohedral β phase at ambient pressure for 23.9–43.8 K, the change in tilt angle of the precession motion occurs for 26–42 K [12]. The corresponding anomalies have been confirmed in the temperature dependence of the vibron bandwidth of Raman scattering [42]. The β phase is magnetically characterized as a two-dimensional

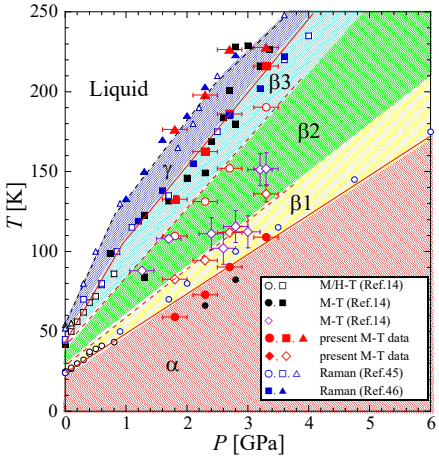

FIG. 3: (Color online) Phase diagram for O_2 physisorbed into SBA-15 with $D = 6.5$ nm, compared with results of previous studies for O_2 without using nanopores [15]. The present study enabled the phase boundary between the liquid and γ phases to be determined through the magnetization for the first time. The phase boundaries are illustrated with the present data in addition to the results of the Raman experiments (open light-blue triangle [44], closed light-blue triangle [45]); the β phase is categorized into three regions: $\beta 1$, $\beta 2$, and $\beta 3$. According to a previous study involving Raman scattering experiments at ambient pressure , three regions in the β phase were related with the change in the vibron bandwidth [1, 42].

short-range order phase. The physisorption into the pores of SBA-15 enabled the change in the tilt angle of the precession motion to appear as a change in the magnetization. Consequently, we can classify the β phase into three regions: $\beta 2$ with a prominent change in the tilt angle of the precession motion; and $\beta 1$ and $\beta 3$ without that over the pressure range up to 3.3 GPa.

B. $D = 8.5 - 24.0$ nm

Figures 4, 5, and 6 show the T dependence of M for O_2 physisorbed into the SBA-15 with $D = 8.5$, 14.5, and 24.0 nm, respectively. For $D = 8.5$ nm, both the β–γ and γ-liquid transition can be traced over all data for 0.7–3.3 GPa, whereas the α–β transition and one anomaly in the β phase were observed for $P \geq 1.8$ GPa. For $D = 14.5$ nm, both α–β and β–γ transitions can be traced throughout the data for 0.7–3.2 GPa, and the γ-liquid transition was observed for $P \geq 1.7$ GPa. For $D = 24.0$ nm, both the β–γ and γ-liquid transitions can be traced throughout the data for 1.6–3.3GPa, whereas the α–β transition was observed for $P \geq 2.2$ GPa. In all data for $D = 24.0$ nm, the β–γ and γ-liquid transitions for noncompressed oxygen molecules in a few rarely physisorbed pores were observed at approximately 50 K. We supposed that with increasing D, the deviation between the fully physisorbed

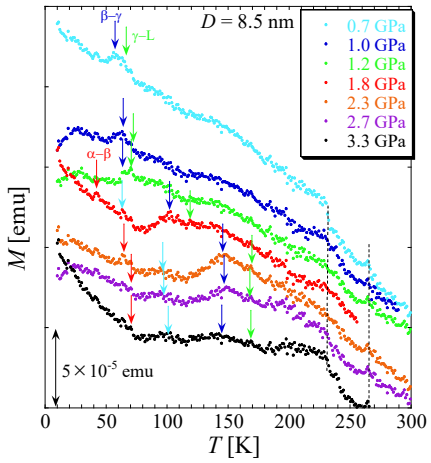

FIG. 4: (Color online) T dependence of M for oxygen molecules physisorbed into SBA-15 with $D = 8.5$ nm. Characteristic temperatures for the α–β transition, one of two well-unknown anomalies in the β phase, β–γ transition, and γ-liquid transition are represented in red, light blue, blue, and green arrows, respectively.

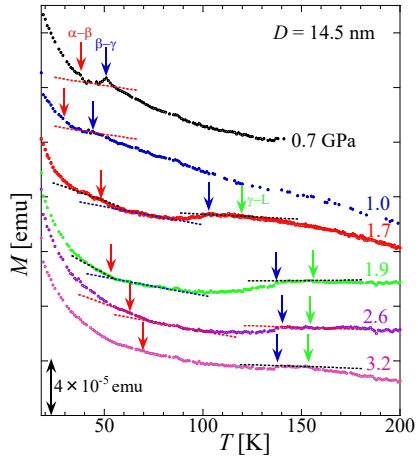

FIG. 5: (Color online) T dependence of M for oxygen molecules physisorbed into SBA-15 with $D = 14.5$ nm. Characteristic temperatures for the α–β, β–γ, and γ-liquid transitions are represented in red, blue, and green arrows, respectively.

and rarely physisorbed states appeared to be prominent.

Figure 7(a) shows the phase diagram of molecule condensation for O_2 physisorbed into the SBA-15 with $D =$ 8.5, 14.5, and 24.0 nm as a function of P and T. Data for $D = 6.5$ nm were included as well. Among a series of transitions, the anomaly due to the β–γ transition exhibited the most significant change in magnetization. At approximately around 2 GPa, all of the four experiments indicated almost the same β–γ transition temperature. It is noteworthy that the change in pressure as a function of T above 2 GPa need not be considered. Figure 7(b) shows

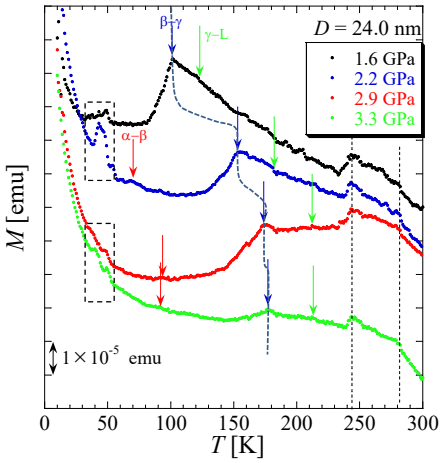

FIG. 6: (Color online) T dependence of M for oxygen molecules physisorbed into SBA-15 with $D = 24.0$ nm. Characteristic temperatures for α–β, β–γ, and γ-liquid transitions are represented in red, blue, and green arrows, respectively. In all data, anomalies appeared at approximately 50 K (shown as broken rectangles), which were likely due to β–γ and γ-liquid transitions for noncompressed oxygen molecules in a few rarely physisorbed pores.

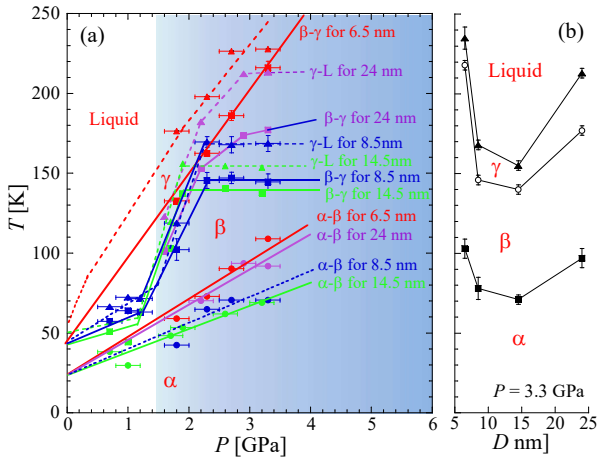

FIG. 7: (Color online) (a) Phase diagram of condensation state of O_2 rods with $D = 8.5$, 14.0, and 24.0 nm. For reference, the phase diagram for $D = 6.5$ nm is shown. To identify any meaningful compression effects, the present results for $P \geq 1.4$ GPa (hatched region with dark yellow) were evaluated as the P value depended significantly on T for low $P_{\rm rt}$. The phase boundaries for $D = 6.5$ and 24.0 nm are close to those for bulk system (see Fig. 3). The O_2 rods with $D =$ 8.5 nm and 14.5 nm exhibit unique phase boundaries. (b) D dependence of phase boundaries in the O_2 condensation at P = 3.3 GPa.

the D dependence of phase boundaries in the O_2 condensation at $P = 3.3$ GPa. There is any D dependence in the molecule condensation phenomenon under compression. Below, by observing the change in the phase boundary

between the β and γ phases for $P > 2$ GPa, we predict the variation in the phase diagram as a function of D.

[1] When $D = 6.5 \rightarrow 8.5$ nm, the phase boundary between the β and γ phases (termed β–γ boundary) shifted toward the low-temperature side. The β–γ transition temperature at $D = 6.5$ nm increased with pressure, whereas at $D = 8.5$ nm, the β–γ boundary did not vary with pressure. For reference, in the study of compression effects on $LaMnO_3$ ($D = 10$ nm) [33] and NiO ($D > 8.6$ nm) nanocrystals [34] synthesized in nanoporous SBA-15, their nanocrystals were strained even at small pressures below 1 GPa. Furthermore, the contraction was anisotropic owing to the one-dimensional cavity. Now, in O_2 physisorbed into the SBA-15 with $D = 6.5$ nm, we have no structural information on the contraction of SBA-15 itself, whereas on the basis of the magnetic information, we could help recognizing that the hydrostatic contraction for the O_2 nanorod was realized there. Considering the information obtained for the $LaMnO_3$ and NiO nanocrystals, we assumed that the compression manner changed from that in Fig. 8(a) to that shown in Fig. 8(b) when D was increased from 6.5 to 8.5 nm. Under the anisotropic compression at $D = 8.5$ nm, the stabilization of solidification by compression would be restricted.

[2] When $D = 8.5 \rightarrow 14.5$ nm, the aforementioned change occurred more easily, and the β–γ boundary shifted slightly toward the lower temperature side. The frozen β–γ boundary for $P > 2$ GPa was strengthened at $D = 14.5$ nm.

[3] When $D = 14.5 \rightarrow 24.0$ nm, the β–γ boundary shifted toward the higher temperature side. At $D = 24.0$ nm, the β–γ transition temperature increased with pressure, whereas it did not reach the β–γ boundary at $D = 6.5$ nm. The α–β boundary at $D = 24.0$ nm was almost consistent with that at $D = 6.5$ nm. They suggest that the compression manner may change toward the hydrostatic-like type.

The solid phase of O_2 at the lower temperature side has lower structural symmetry. A series of present experimental results revealed that the change in magnetic property was related to the change in the crystal structure. The indirect compression of O_2 condensed via the compression of molecular physisorption media with D around 10 nm promoted an anisotropic shrinkage of O_2 networks. The pressure dependence of the β–γ boundary that appeared at $D = 8.5$ and 14.5 nm for $P > 2$ GPa revealed that anisotropic shrinkage did not thermally encourage the solid phase under a compressed environment.

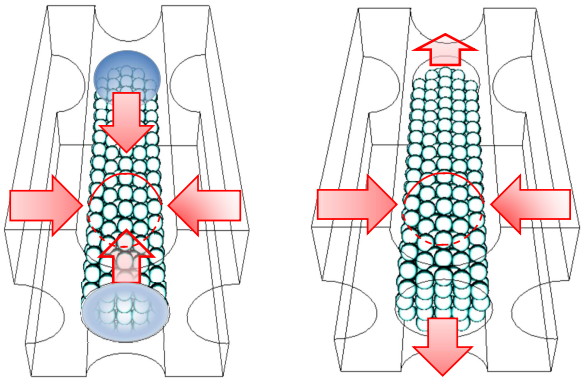

FIG. 8: (Color online) Change in frame of O_2 condensation in SBA-15 for (a) $D = 6.5$ nm and (b) $D \geq 8.5$ nm. Here, D is the diameter of the nanopores in SBA-15. The number of O_2 was reduced for simplicity. For a small D such as (a), quasi-hydrostatic compression was realized because of the blockade of pore edges. When the porous blockade at the edges was insufficient, the nanorod elongated along the long axis and shortened along the radial direction, as shown in (b). $LaMnO_3$ ($D = 10$ nm) and NiO ($D \geq 8.6$ nm) nanocrystals synthesized in the nanopores of SBA-15 were assumed to exhibit the compression style shown in (b) [33, 34].

IV. CONCLUSION

We conducted two types of compression experiments for a condensed O_2 network physisorbed into the nano-sized pores of SBA-15 with $D = 6.5$. 8.5, 14.0, and 24.0 nm. For $D = 6.5$ nm, hydrostatic contraction was facilitated by the help of high physisorption capacity. Furthermore, we experimentally elucidated the rich magnetic properties of condensed O_2. Utilizing prominent adsorption nature in nanometer porous medium, the phase boundary between γ-liquid phases was determined on the basis of magnetization data. The change in precession angle in the β phase was investigated at high pressure up to 3.3 GPa, in which the β phase was categorized into three regions. The anisotropic compression effects on the condensed O_2 system were investigated for $D = 8.5$, 14.0, and 24.0 nm. It was discovered that their phase diagrams differed from those under hydrostatic compression. The condensed state of O_2 molecules, which is a gas at room temperature and ambient pressure, is variable by the directivity of the change in the molecular network as well as the stress magnitude.

V. DATA AVAILABILITY STATEMENT

The data that supports the findings of this study are available within the article.

[1] Y. A. Freiman and H. J. Jodl, Phys. Rep. **401**, 1 (2004).
[2] F. Haldane, Phys. Lett. A **93**, 464 (1983).
[3] M. Faraday, *Experimental Researches in Electricity, Series XXV Vol. 3* (Taylor and Francis, London, 1855).
[4] J. Dewa, Proc. Roy. Soc. (London) A **50**, 10 (1891).
[5] H. K. Onnes and A. Perrier, Comm. Phys. Lab. Leiden **116**, 1 (1910).
[6] A. Borovik-Romanovl, Zh. Exp. Theor. Fiz. **21**, 1303 (1951).
[7] E. Kanda, T. Haseda, and A. Otsubo, Physica **20**, 131 (1954).
[8] G. DeFotis, Phys. Rev. B **23**, 4714 (1981).
[9] R. J. Meier, C. J. Schinkel, and A. de Visser, J. Phys. C: Solid State Phys **15**, 1015 (1982).
[10] C. Uyeda, K. Sugiyawa, and M. Date, J. Phys. Soc. Jpn. **54**, 1107 (1985).
[11] Y. A. Freimanl, H. J. Jodl, and Y. Crespo, Phys. Rep. **743**, 1 (2018).
[12] J. Laufer and G. Leroi, J. Chem. Phys. **55**, 993 (1971).
[13] H. Roder, J. Phys. Chem. Ref. Data **7**, 949 (1978).
[14] T. Nomura, Y. Matsuda, S. Takeyama, A. Matsuo, K. Kindo, J. Her, and T. C. Kobayashi, Phys. Rev. Lett. **112**, 247201 (2014).
[15] M. Mito, S. Yamaguchi, H. Tsuruda, H. Deguchi, and M. Ishizuka, J. Appl. Phys. **115**, 13903 (2014).
[16] S. Desgreniers, Y. Vohra, and A. Ruoff, J. Appl. Cryst. **94**, 1117 (1990).
[17] Y. Akahama and H. Kawamura, Phys. Rev. B **61**, 8801 (2000).
[18] G. Weck, P. Loubeyre, and R. LeToullec, Phys. Rev. Lett. **88**, 035504 (2002).
[19] A. Goncharov, E. Gregoryanz, R. Hemley, and H. Mao, Phys. Rev. B **68**, 100102 (2003).
[20] Y. Akahama, H. Kawamura, D. Häusermann, M. Hanfland, and O. Shimomura, Phys. Rev. Lett. **74**, 4690 (1995).
[21] G. Weck, S. Desgreniers, P. Loubeyre, and M. Mezouar, Phys. Rev. Lett. **102**, 255503 (2009).
[22] K. Shimizu, K. Suhara, M. Ikumo, M. Eremets, and K. Amaya, Nature **393**, 767 (1998).
[23] I. N. Goncharenko, Phys. Rev. Lett. **94**, 205701 (2005).
[24] U. Kobler and R. Marx, Phys. Rev. B **35**, 9809 (1987).
[25] Y. Murakami and H. Suematsu, Phys. Rev. B **54**, 4146 (1996).
[26] Y. Murakami, J. Phys. Chem. Solid **59**, 467 (1998).
[27] W. Mori, T. C. Kobayashi, J. Kurobe, K. Amaya, Y. Narumi, T. Kumada, K. Kindo, H. A. Katori, T. Goro, N. Miura, et al., Mol. Cryst. Liq. Cryst. **306**, 1 (1997).
[28] R. Kitaura, S. Kitagawa, Y. Kubota, T. C. Kobayashi, K. Kindo, Y. Mita, A. Matsuo, M. Kobayashi, H.-C. Chang, T. C. Ozawa, et al., Science **298**, 2358 (2002).
[29] T. C. Kobayashi, A. Matsuo, M. Suzuki, K. Kindo, R. Kitaura, R. Matsuda, and S. Kitagawa, Prog. Theor. Phys., Suppl. **159**, 271 (2005).
[30] S. Takamizawa, E. Nakata, and T. Akatsuka, Angew. Chem. Int. Ed. **118**, 2274 (2006).
[31] M. Mito, N. Shinto, Y. Komorida, T. Tajiri, H. Deguchi, S. Takagi, and S. Kohiki, Phys. Rev. B **78**, 064428 (2008).
[32] T. Tajiri, S. Saisho, M. Mito, H. Deguchi, K. Konishi, and A. Kohno, J. Phys. Chem. C **119**, 1194 (2015).
[33] T. Tajiri, S. Saisho, Y. Komorida, M. Mito, H. Deguchi, and A. Kohno, J. Appl. Phys. **110**, 044307 (2011).
[34] M. Mito, T. Tajiri, S. Saisho, H. Deguchi, A. Kohno, and K. Nakamura, J. Magn. Magn. Mater. **489**, 165407 (2019).
[35] M. Mito, M. Hitaka, T. Kawae, K. Takeda, T. Kitai, and N. Toyoshima, Jpn. J. Appl. Phys. **40**, 6641 (2001).
[36] M. Mito, J. Phys. Soc. Jpn. Suppl. A **76**, 182 (2007).
[37] K. Takeda and M. Mito, J. Phys. Soc. Jpn. **71**, 729 (2002).
[38] M. Ohba, W. Kaneko, S. Kitagawa, T. Maeda, and M. Mito, J. Am. Chem. Soc. **130**, 4475 (2008).
[39] M. Mito, K. Matsumoto, Y. Komorida, H. Deguchi, S. Takagi, T. Tajiri, T. Iwamoto, T. Kawae, M. Tokita, and K. Takeda, J. Phys. Chem. Solid **70**, 1290 (2009).
[40] G. Subias, V. Cuartero, J. Garcia, J. Blasco, S. Lafuerza, S. Pascarelli, O. Mathon, C. Strohm, K. Nagai, M. Mito, et al., Phys. Rev. B **89**, 094408 (2013).
[41] G. J. Piermarini, S. Block, J. D. Barnett, and R. A. Forman, J. Appl. Phys. **46**, 2774 (1975).
[42] J. Kreutz and H. Jodl, Phys. Rev. B **68**, 214303 (2003).
[43] H. Hochheimer, H. J. Jodl, W. Henkel, and F. Bolduan, Chem. Phys. Lett. **106**, 79 (1984).
[44] H. J. Jodl, F. Bolduan, and H. D. Hochheimer, Phys. Rev. B **31**, 7376 (1985).
[45] J. Yen and M. Nicol, J. Appl. Cryst. **91**, 3336 (1987).